THE JOURNAL OF PHYSICAL CHEMISTRY B

Article

Cite This: J. Phys. Chem. B 2019, 123, 8717−8726

pubs.acs.org/JPCB

Influence of Hydrogen Bonds on the Electron−Phonon Coupling Strength/Marker Mode Structure and Charge Separation Rates in Reaction Centers from *Rhodobacter sphaeroides*

Anton Khmelnitskiy,[†,⊥] JoAnn C. Williams,[§] James P. Allen,[§] and Ryszard Jankowiak*[,†,‡]

[†]Department of Chemistry and [‡]Department of Physics, Kansas State University, Manhattan, Kansas 66506, United States

[§]School of Molecular Sciences, Arizona State University, Tempe, Arizona 85287, United States

Supporting Information

ABSTRACT: Low-temperature persistent and transient hole-burning (HB) spectra are presented for the triple hydrogen-bonded L131LH + M160LH + M197FH mutant of *Rhodobacter sphaeroides*. These spectra expose the heterogeneous nature of the P-, B-, and H-bands, consistent with a distribution of electron transfer (ET) times and excitation energy transfer (EET) rates. Transient $P^+Q_A^-$ holes are observed for fast (tens of picoseconds or faster) ET times and reveal strong coupling to phonons and marker mode(s), while the persistent holes are bleached in a fraction of reaction centers with long-lived excited states characterized by much weaker electron−phonon coupling. Exposed differences in electron−phonon coupling strength, as well as a different coupling to the marker mode(s), appear to affect the ET times. Both resonantly and nonresonantly burned persistent HB spectra show weak blue- (∼150 cm^{-1}) and large, red-shifted (∼300 cm^{-1}) antiholes of the P band. Slower EET times from the H- and B-bands to the special pair dimer provide new insight on the influence of hydrogen bonds on mutation-induced heterogeneity.

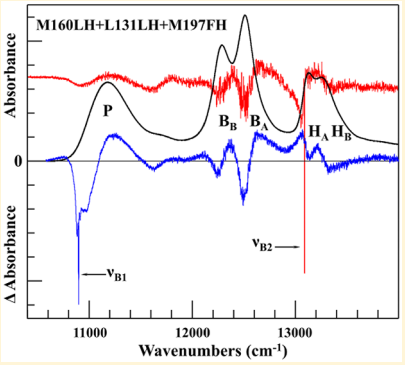

1. INTRODUCTION

Photosynthesis, the main source of energy for life on Earth, converts solar radiation into chemical energy via multistep processes.[1] Solar photons are absorbed by membrane-associated antenna complexes, and excitation energy is efficiently transferred to the reaction center (RC) where it is used to drive charge separation (CS). The RC in bacterial photosynthesis (bRC) is a membrane-bound pigment−protein complex that performs the primary photochemistry.[2,3] In the bRC from *Rhodobacter (Rb.) sphaeroides*, light absorption by a special pair bacteriochlorophyll dimer, P, initiates the transfer of an electron through the intermediate electron acceptors (B_A and H_A) to the primary quinone, Q_A, and then the secondary quinone, Q_B. The electronic structure, excitation energy transfer (EET), and charge separation (CS) dynamics of wild type (WT) and mutant bRCs have been intensely characterized.[4−10] The influence of amino acids and various mutations in the vicinity of the special pair bacteriochlorophyll a (BChl) comprising the so-called P-band (P_A/P_B) in the bRC of *Rb. sphaeroides* has been widely studied via Stark, Fourier transform infrared, Fourier transform Raman, electron paramagnetic resonance, electron nuclear double resonance, and time-domain spectroscopies.[11−18] In contrast to the predominance of these experiments being performed at room temperature or 77 K, we present low-temperature results (T = 4 K) of site selective (high-resolution) persistent (nonphotochemical) and transient (photochemical) hole-burning (HB) data to provide insights on the primary CS, electron−phonon coupling (el−ph), and energy landscape.

The structural arrangement of the chromophores in WT and mutant bRCs is well-known.[19−24] In the WT bRCs, there is only one H-bond between the carbonyl group on the P_A molecule and histidine L168, but additional hydrogen bonds can be introduced by mutagenesis of the surrounding protein.[11,12,25,26] In particular, the triple mutant of *Rb. sphaeroides* (L131LH + M160LH + M197FH) has all four carbonyl groups of the special pair hydrogen (H)-bonded by the substitution of leucine at M160 and L131 and phenylalanine at M197 with histidines (Figure 1).[23,27] As the H-bonds are introduced, the unpaired electron of P^+ can be gradually shifted from a predominant localization on P_A to a localization on P_B depending on the number of H-bonds.[27,28] Moreover, the addition of each H-bond in the BChl dimer is correlated with an increase in the oxidation/reduction potential of the dimer.[26] The most extreme increase in midpoint potential was observed in the *Rb. sphaeroides* triple H-bond mutant, i.e., 260 mV higher than in WT bRCs.[26,29] The triple mutant has much slower electron transfer (ET) and distribution of ET times for the primary CS than WT.[29,30] We anticipate that in addition to transient holes observed via the $P^+Q_A^-$ bottleneck state, we should also observe persistent HB spectra that could reveal if changes in the primary electron

Received: September 3, 2019
Published: September 20, 2019

DOI: 10.1021/acs.jpcb.9b08388
J. Phys. Chem. B 2019, 123, 8717−8726

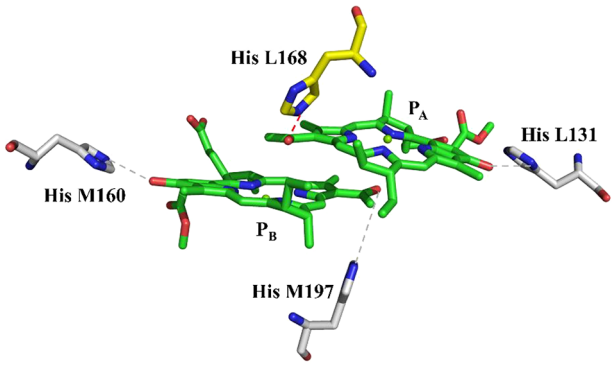

Figure 1. Special pair arrangement of BChls (P_A and P_B) based on the X-ray structure of the RC from *Rb. sphaeroides* (PDB ID 2J8C).[24] Positions of His side chains substituted by site-directed mutagenesis are shown schematically. H-bonds between imidazole groups of His L131/M160 and keto carbonyl groups of P_A/P_B and H-bond between His M197 and acetyl carbonyl group of P_B in the triple mutant are indicated schematically by the gray dashed lines. The H-bond between the P_A BChl and His L168 present in the WT bRC is schematically shown by the red dashed line.

donor mode structure are present. The latter could also provide insight into the energy landscape in bRCs with very slow CS kinetics. Additionally, site selective spectroscopy could reveal if this triple mutation affects the excitation energy transfer (EET) from the B- and/or H-band to the primary donor state P. Although we focus on various 4 K optical HB spectra, whenever it was necessary to advance our interpretation, a comparison with spectra obtained for the single mutants (L131LH, M160LH, and M197FH) was also made.

Presented here are high-resolution, low-temperature (T = 4 K) HB spectra that examine how environmental perturbation(s) (via formation of additional H-bands to the special pair BChls) affect disorder (heterogeneity), el−ph coupling, EET/ET times, and coupling to special pair marker mode(s). The results show that the 4 K HB spectroscopy provides more insight into modified dynamics present in the triple mutant, revealing mutation-induced heterogeneity. We discuss the shape of transient and persistent bleaches due to the modified electronic structure and the distribution of CS kinetics. Our data lead to new insights into mutation-induced effects in BRCs. A theoretical description of the absorption and HB spectra will be reported elsewhere.

2. MATERIALS AND METHODS

2.1. Preparation of Mutants. All mutants studied in this work were prepared as described previously.[31] Briefly, the single and triple mutants were constructed by oligonucleotide-directed mutagenesis and cloning of restriction framgents.[11,12] Reaction centers were isolated from semiaerobically grown cultures.[11,26,32] After isolation, the reaction buffer consisted of 15 mM Tris-HCl, pH 8.0, and 0.05% Triton X-100.

2.2. Instrumentation. For low-temperature experiments, samples were diluted with 45:55 (v/v) buffer:glass solution. The glass-forming solution was 55:45 (v/v) glycerol:ethylene glycol. Details about the measurement setup were described elsewhere.[33] Briefly, a Bruker HR125 Fourier transform spectrometer was used to measure the absorption and HB spectra with resolutions of 4 and 2 cm^{-1}, respectively. Excitation (488.0 nm) for nonresonant HB (NRHB) spectra was produced from a Coherent Innova 200 argon ion laser. Selectively excited bleaches (via tunable wavelengths) were obtained from a Coherent CR899 Ti:sapphire laser (laser line width 0.07 cm^{-1}) pumped by a Spectra-Physics Millennia Xs diode laser (532 nm). Laser power in all experiments was precisely set by a continuously adjustable neutral density filter. Low-temperature (4 K) experiments were performed using an Oxford Instruments Optistat CF2 cryostat with sample

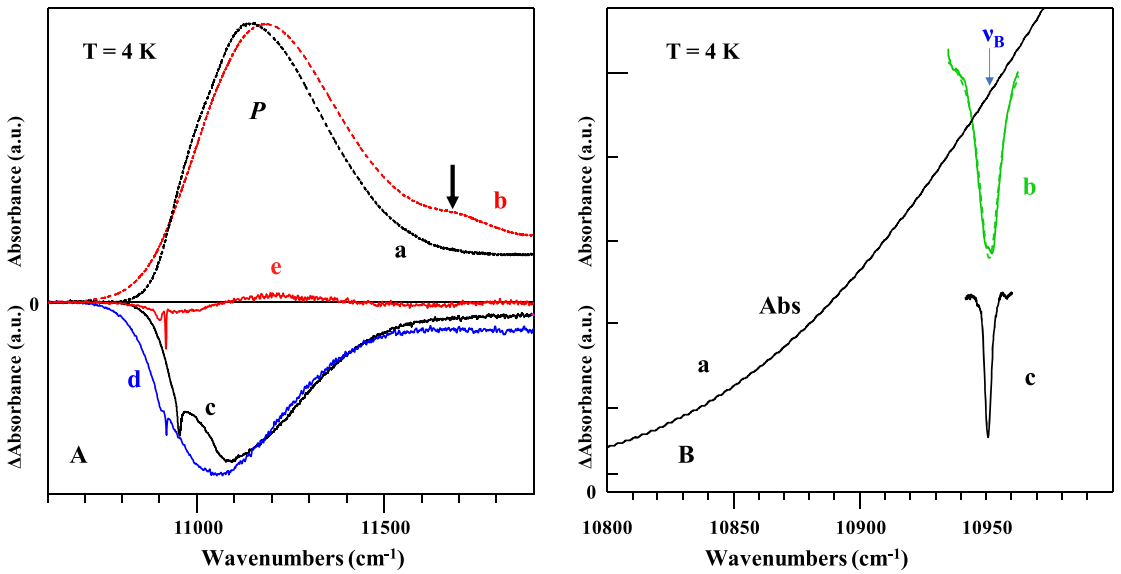

Figure 2. (A) Spectra a/c and b/d (T = 4 K) show the P-band absorption/resonant transient HB spectra obtained for WT bRC of *Rb. sphaeroides* and the triple mutant (L131LH + M160LH + M197FH), respectively. Spectra c and d are obtained with burning frequency of ν_{B2} = 10 953 cm^{-1} and ν_{B1} = 10 917 cm^{-1}, respectively. Curve e is persistent hole obtained at burning frequency (ν_{B1}) of 10 917 cm^{-1}. (B) Low-energy wing of the triple mutant absorbance and two extracted (transient) ZPHs. Holes b and c in this frame were burned at very similar frequencies; i.e., ν_B = 10 951 cm^{-1} (λ_B = 913.2 nm) and ν_B = 10 953 cm^{-1} (λ_B = 913.0 nm) for the WT bRC and the triple mutant, respectively. The Lorentzian fit of curve b is shown as dashed line (read resolution = 2 cm^{-1}).

DOI: 10.1021/acs.jpcb.9b08388
J. Phys. Chem. B 2019, 123, 8717−8726

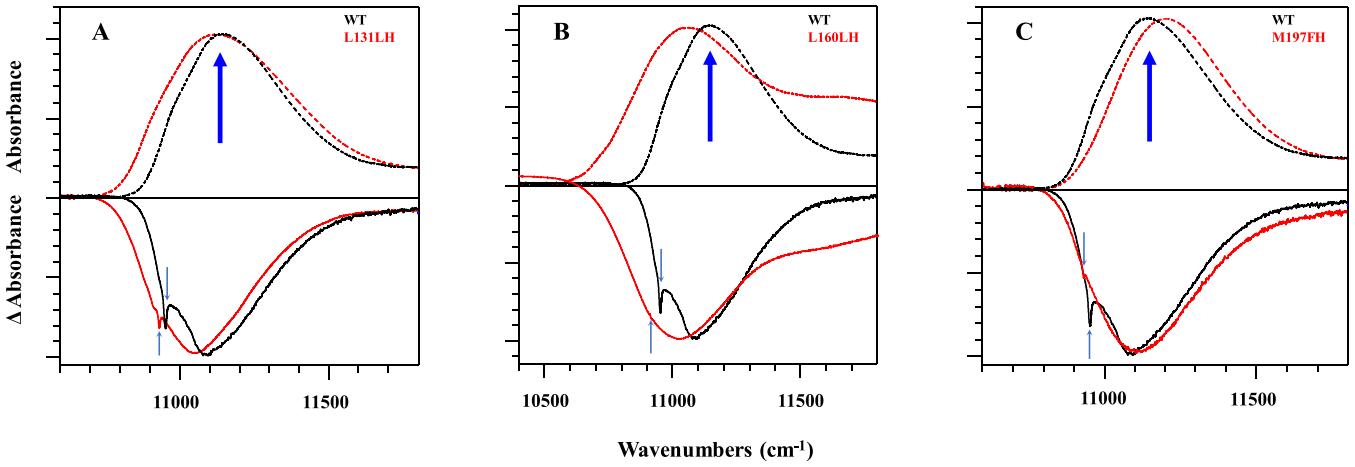

Figure 3. Normalized P-band absorption and transient HB spectra for WT bRC (black spectra) compared with spectra obtained for three individual mutants (L131LH, frame A; L160LH, frame B; and M197FH, frame C); red spectra.

temperature read and controlled by a Mercury iTC temperature controller.

2.3. Spectroscopic Methodologies. The hole-burning (HB) spectroscopy relies on differences observed in the absorption spectrum of a low-temperature system after narrowband laser excitation. If a pigment molecule (in resonance with the laser) experiences photochemical reaction, it ceases to absorb at its original wavelength/frequency, and one speaks of photochemical HB (PHB). In the case of nonphotochemical HB (NPHB), the pigment molecule does not undergo a chemical reaction, but its immediate environment experiences some rearrangement (for more details see refs 34 and 35). Both PHB and NPHB may result in the formation of persistent holes, meaning the holes are preserved after the initial excitation is turned off, as long as low temperature is maintained. In either case, the HB spectrum is obtained as the difference between the measured absorption spectrum before and after laser excitation. Generation of transient HB spectra requires the presence of a third, relatively long-lived state. That is, the excited state evolves into a triplet state or is converted photochemically to another long-lived (microsecond to millisecond range) product (e.g., a charge-separated state $P^+Q_A^-$), leaving a transient hole in the absorption spectrum with a zero-phonon hole (ZPH) at the frequency of the original excitation (resonant HB) and with shape defined by the strength of electron−phonon (el−ph) coupling. In this case, the pigment's ground state is depopulated for the lifetime of the long-lived state, and the spectral hole will be observable only for the duration of this lifetime. The transient holes discussed in this work are acquired as the difference between the absorption spectra measured while the excitation is on and off (postburn absorption, i.e., after saturation of a persistent hole).

Nonresonant holes are obtained for excitation of high-energy pigments or high-energy spectral bands. In this case, radiationless EET takes place from high-energy pigment(s) to the low-energy pigment(s) or from higher energy states (excitons) to the lowest energy pigment(s) or state. In general, EET occurs from a manifold of vibrational states, associated with the excited electronic state of the donor molecule, into a manifold of vibrational states associated with the ground state of the acceptor molecule. The key information provided by HB spectroscopy (relevant to data discussed below) includes lifetimes of the zero-point level of $S_1(Q_y)$-states due to EET and/or ET, as determined by the widths of ZPH and el−ph (protein) coupling parameter. For more details on HB spectroscopy, see refs 34−36.

3. RESULTS

3.1. Absorption and Transient HB Spectra. Resonant (transient) holes burned into the lowest-energy state of bRCs provide information on interaction of low-energy pigments (i.e., special pair BChls) with the protein environment. Figure 2A compares the P-band absorption obtained for the triple mutant (curve b) and a representative transient $P^+Q_A^-$ HB spectrum (curve d). The latter curve was burned resonantly within the P-band at 4 K (ν_{B1} = 10 917 cm^{-1}). Curve e is a persistent hole burned at the same frequency that will be discussed below (see Figure 5). The black spectra (absorption, curve a) and transient $P^+Q_A^-$ hole (curve c) were obtained for the wild-type (WT) bRC and are shown for comparison. As mentioned above the shape of HB spectrum depends on the strength of el−ph coupling. Different shapes and bandwidths of these spectra clearly indicate that the triple mutation affects the special pair disorder and/or el−ph coupling strength/special pair marker mode progression (vide infra).

The same types of spectra as those shown in Figure 2A obtained for the three single-point mutants: L131LH, L160LH, and M197FH are shown for comparison in Figure 3 (red spectra); these spectra are also compared with the same types of spectra obtained for the WT *Rb. sphaeroides* (black curves). For completeness the low-temperature absorption spectra of single and triple mutants, in a much broader spectral range (10 600−14 000 cm^{-1}), are shown in Figure S1 of the Supporting Information and will be used in future modeling studies. These spectra illustrate that spectral changes occur not only within the P-band but also in the B- and H-bands. However, in this work we focus on the nature of the P-bands. To provide more insight into the 11 700 cm^{-1} band indicated by the thick arrow in Figure 2A (referred below to the P′-band), Figure 3 compares the P-band absorption and (resonant) transient HB spectra obtained for the WT bRC (dashed and solid black curves, respectively) with the same types of spectra obtained for three single mutants (red spectra), i.e., the L131LH (frame A), M160LH (frame B), and M197FH (frame C) mutants, respectively.

DOI: 10.1021/acs.jpcb.9b08388
J. Phys. Chem. B 2019, 123, 8717−8726

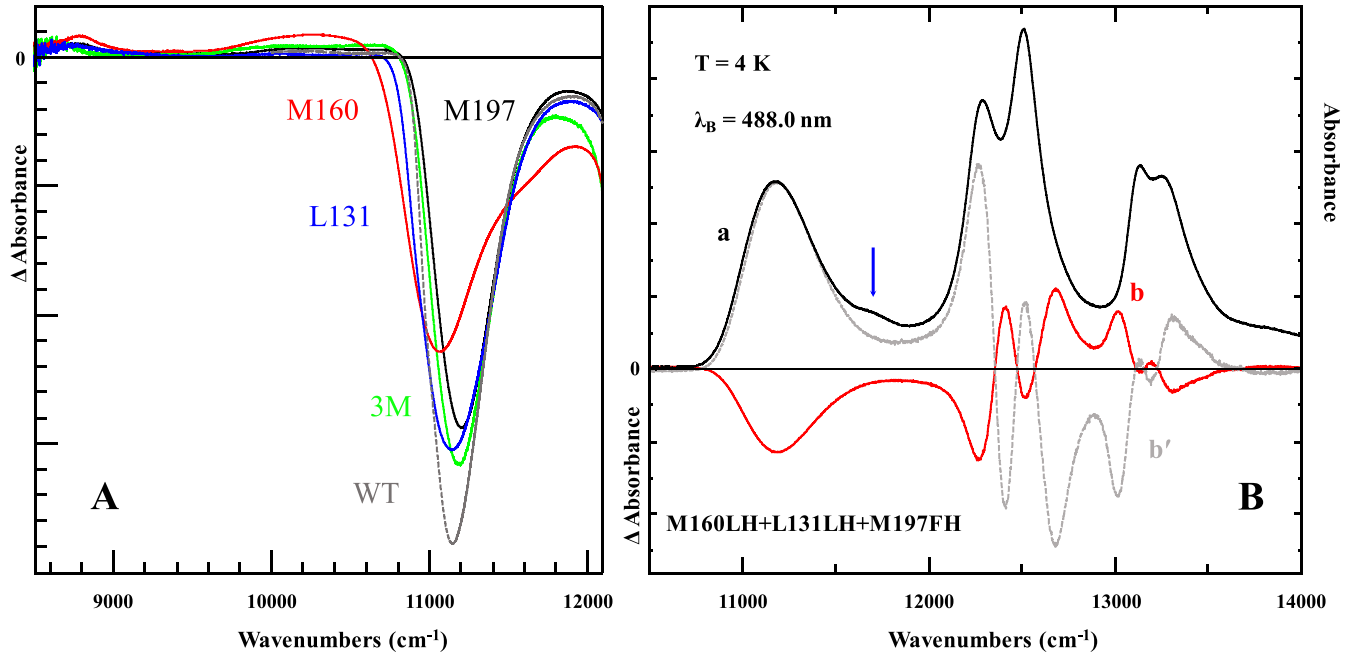

Figure 4. (A) Normalized nonresonant transient $P^+Q_A^-$ spectra of WT bRCs, the triple mutant (3M), and three single mutants: L131LH mutant (L131), M160LH (M160), and M197FH (M197). (B) Absorption (curve a) and nonresonant transient $P^+Q_A^-$ HB spectrum (curve b) obtained for the triple mutant (L131LH + M160LH + M197FH). The gray curve b′ spectrum is the inverted curve b. Burning frequency ν_B = 20 492 cm^{-1} (λ_B = 488.0 nm); T = 4 K.

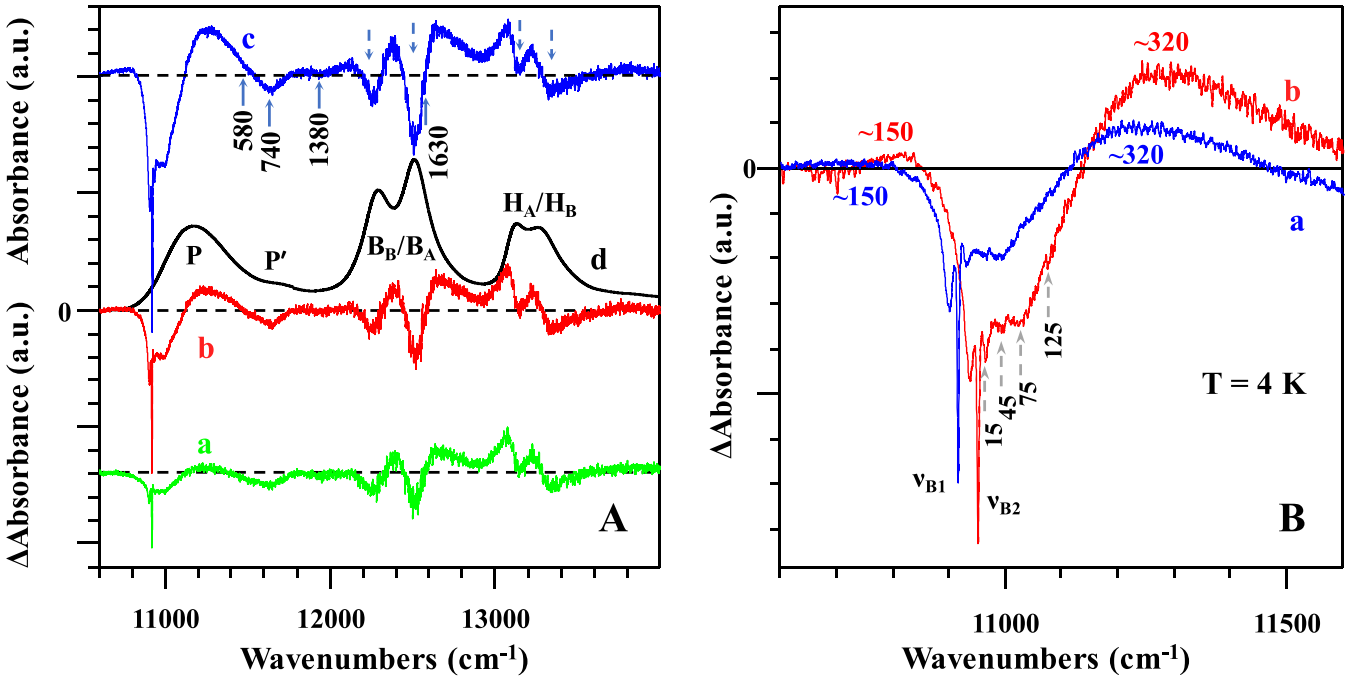

Figure 5. (A) Persistent HB spectra (ν_{B1} = 10 917 cm^{-1}; T = 4 K) burned at f of 30 J/cm^2 (a), 127 J/cm^2 (b), and 570 J/cm^2 (c), respectively, in the triple mutant. The dashed black lines show ΔA = 0. The downward dashed arrows indicate satellite holes bleached within the B and H bands. The blue upward arrows label possible vibronic states. Spectrum d is the 4 K absorption spectrum. (B) Expanded persistent HB spectra within the P-band obtained at ν_{B1} = 10 917 cm^{-1} (curve a; f = 127 J/cm^2) and ν_{B1} = 10 950 (curve b; f = 325 J/cm^2). Spectra a–c in frame A are offset for clarity. All numbers are in cm^{-1}. See text for details.

The thin blue arrows in the transient HB spectra shown in Figure 3 indicate burning frequencies (ν_B). The thick upward blue arrows indicate the maximum of the WT bRC absorption spectrum. All spectra were obtained at T = 4 K. The largest absorption changes are observed for the L160LH mutant (see frame B) that also shows an additional absorption band located between the P and B bands near 11 700 cm^{-1} (or equivalently 854.7 nm) that was designated above (at least in part) as the P′-band. Similar band, though notably weaker, is also observed in the triple mutant (see curve b in Figure 2A); see section 3.1 for more details. Low-temperature transient (nonresonant) $P^+Q_A^-$ holes of the WT, the triple mutant, and three single

DOI: 10.1021/acs.jpcb.9b08388
J. Phys. Chem. B 2019, 123, 8717–8726

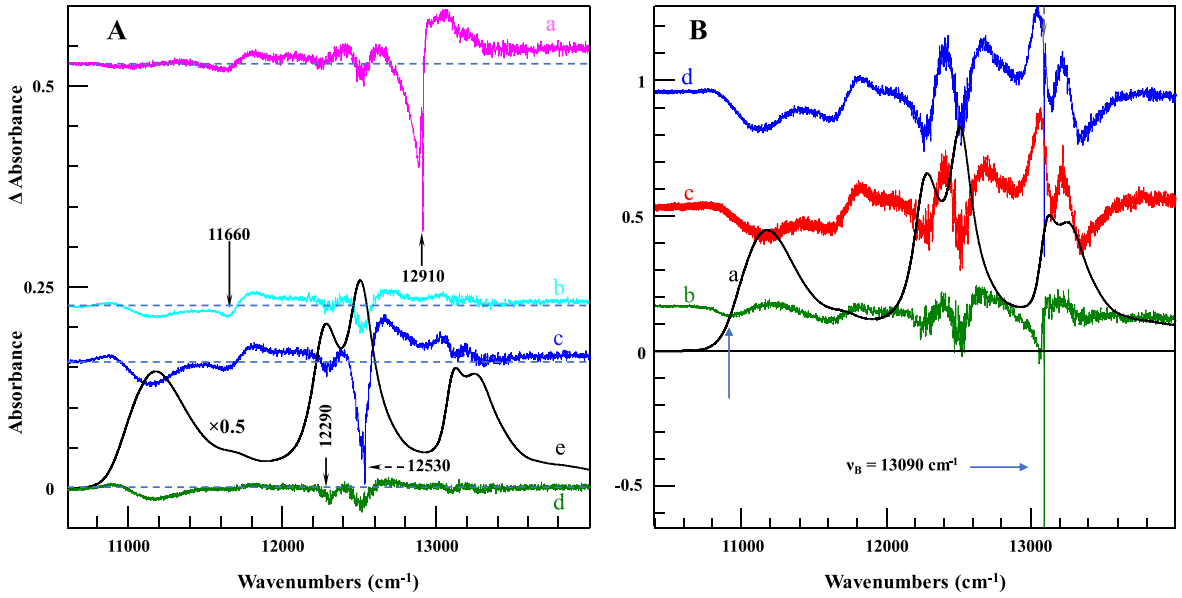

Figure 6. (A) Persistent hole-burned spectra, multiplied by 100, burned at 774.6 nm (ν_B = 12 910 cm^{-1}, fluence = 93 J/cm^2) (curve a), 857.6 nm (ν_B = 11 660 cm^{-1}, fluence = 380 J/cm^2) (curve b), 798 nm (ν_B = 12 530 cm^{-1}, fluence = 190 J/cm^2) (curve c), and 813.7 nm (ν_B = 12 290 cm^{-1}, fluence = 144 J/cm^2) in the triple mutant. Curve e is the absorption spectrum of the triple mutant. (B) Triple-mutant absorption spectrum (curve a). Persistent holes (multiplied by a factor of 100) are burned at 764 nm (13 090 cm^{-1}, fluence = 12 J/cm^2) (b) and 488 nm (20 490 cm^{-1}, fluence = 55 J/cm^2; curve c). Curve (d) was obtained by simultaneous burning at 13 090 and 20 490 cm^{-1} with the fluence of 12 and 54 J/cm^2, respectively.

mutants obtained for ν_B = 20 492 cm^{-1} (λ_B = 488.0 nm) in the near-infrared spectral region of ∼8 600−12 000 cm^{-1} are shown in Figure 4A. These spectra were normalized at the maximum of the H-band near 13 054 cm^{-1} (∼766 nm) observed in corresponding transient spectra (for the normalization details see Figure S2 in the Supporting Information which shows the same spectra in a much broader spectral range). Regarding the spectra shown in Figure 4A, we note that the major band of the $P^{\bullet+}$ state lies in the near-infrared region near 8000 cm^{-1} (1250 nm).[25] Unfortunately, this region cannot be observed by our FTIR spectrometer. The shapes of the nonresonant 4 K HB spectra, as well as the maxima of the P-bands of all mutants, are very different from the corresponding spectra obtained for the WT bRC (see gray dashed curve in Figure 4A).

For example, the maximum of the P-band of the single L131LH and L160LH mutants is shifted red by 7 and 72 cm^{-1}, respectively, while the P-band of the M197FH and triple mutant (see Figure 2A) is shifted blue by ∼58 and 42 cm^{-1}, respectively. Large differences between the transient $P^+Q_A^-$ HB spectra (both resonant and nonresonant) are also evident (compare data shown in Figures 2A, 3, and 4A). Figure 4B shows the absorption (curve a) and nonresonant (curve b) transient $P^+Q_A^-$ HB spectrum for the triple mutant over a broad range; recall that these data were also obtained at ν_B = 20 492 cm^{-1} (λ_B = 488.0 nm). The gray (curve b′) spectrum is the inverted curve b demonstrating that the band, indicated by the solid arrow near 11 700 cm^{-1} (P′ -band), is not bleached in this spectral region (vide infra).

3.2. Persistent HB Spectra Burned within the P, P′, B, and H-Bands. Before we discuss the persistent (resonant) holes burned within the P-band in the triple mutant, we note that WT bRCs do not exhibit persistent HB due to a highly efficient and fast (∼1 ps) ET time at low temperatures.[3,4] Previous data of frequency-dependent ZPHs observed in transient spectra also suggested a very small (if any) distribution of ET times in WT bRCs.[37] In contrast, persistent holes are observed in the triple mutant; for example, fluence (f)-dependent persistent holes (burned at ν_{B1} = 10 917 cm^{-1}) are shown as curves a−c in Figure 5A. These persistent holes also reveal very complex bleaches within the P-, B-, and H-bands. Spectra a, b, and c in Figure 5A were obtained for f equal to 30, 127, and 570 J/cm^2, respectively.

In Figure 5A the 4 K absorption spectrum (curve d) is shown for comparison with the persistent bleaches observed in spectra a−c. The hole obtained at f = 570 J/cm^2 (see curve c in Figure 5A) is near the saturation limit and carries a hole depth of ∼12%. Figure S4 in the Supporting Information shows the percentage hole depth (for hole burned at ν_B = 10 917 cm^{-1}) plotted as a function of f. Figure 5B shows the expanded bleach within the P-band for two burning frequencies, i.e., ν_{B1} = 10 917 cm^{-1} (curve a; f = 325 J/cm^2) and ν_{B2} = 10 950 cm^{-1} (curve b; f = 127 J/cm^2). In contrast to transient holes, persistent holes reveal deep ZPHs consistent with a weak el−ph coupling. Multiphonon progression (ω_{ph}) with clearly resolved bands near 15, 45, and 75 cm^{-1} is also clearly exposed (see gray dashed arrows in Figure 5B). The very weak shoulder near 125 cm^{-1} could correspond to the slightly modified special pair (sp) marker mode Franck−Condon progression (ω_{sp}), with a significantly smaller Huang−Rhys factor (S_{sp}) in comparison with the WT bRC. Remarkably, similar frequencies were observed in the spectrum of coherent oscillations in kinetics of stimulated emission of P* in the triple mutant at 90 K.[38]

Figure 6 shows persistent HB spectra burned excited at 11 660, 12 290, 12 530, and 12 910 cm^{-1} (frame A) and 13 090 and 20 490 cm^{-1} (frame B). Interestingly, burning in the P′-band (11 660 cm^{-1}; curve b in frame A) produces a broad bleach with a minimum at the burning frequency and a blue-shifted (∼170 cm^{-1}) antihole. The absence of ZPH at the

DOI: 10.1021/acs.jpcb.9b08388
J. Phys. Chem. B 2019, 123, 8717−8726

burning frequency indicates either a short-lived (subpicosecond) excited state or strong el−ph coupling of the corresponding transition. Concomitant bleaching of the P band is relatively weak and most probably caused by excitation of higher energy vibronic transitions of P, suggesting that the P and P′ bands are not connected and, instead, burned independently.

Remarkably, burning within the B_A band at 12 530 cm^{-1} (curve c, frame A) produces both a broad bleach and relatively narrow (hole width $\Gamma_{ZPH} \approx 5.3$ cm^{-1}) ZPH, corresponding to ∼2 ps (corrected for spectral resolution) EET time. We showed earlier that in wild-type bRCs narrow ZPH can be burned within the B-band only if the P-band is oxidized and EET from the B-band to P is blocked.[39] Meanwhile, EET to P-band is observed in our sample as evidenced by its significant bleach under burning at 12 530 cm^{-1}. Interestingly, burning at 13 090 cm^{-1} (curve b) and 20 490 cm^{-1} (curve c) in frame B shows very different bleaches within the P-band (note the blue upward arrow below curve c). Curve d shows the ZPH at 12 530 cm^{-1} and a broad bleach of the entire P-band, since this sectrum was obtained simultaneous burning at 13 090 and 20 490 cm^{-1}. See section 4.4 for more details.

4. DISCUSSION

4.1. P-Band Absorption and Transient HB Spectra. Recall that spectra c (WT bRC; hole depth = 11%) and d (triple mutant; hole depth = 4%) in Figure 2A represent resonant transient $P^+Q_A^-$ spectra obtained at slightly different excitation frequencies, i.e., ν_{B2} = 10 953 cm^{-1} and ν_{B1} = 10 917 cm^{-1}, respectively. Note that the transient bleach in curve d in Figure 2A is also broader than that seen in curve c. Moreover, mutant absorption spectrum (curve b) is broader with a blue-shifted maximum (by ∼40 cm^{-1}); however, the main difference between the P-bands is the presence of an additional absorption band observed in the triple mutant near 11 700 cm^{-1} (854.7 nm), as indicated by the thick arrow (vide infra). Although both transient holes exhibit weak ZPHs at burning frequencies, the ZPH (a sharp spike) observed at ν_{B1} = 10 917 cm^{-1} in the triple mutant (curve d in Figure 2A) is narrower than that in spectrum c burned at ν_{B2}, but its width is resolution limited. This is more clearly illustrated in Figure 2B that shows the extracted ZPHs. The low-energy wing of the triple-mutant absorbance (curve a) is shown for comparison. The Lorentzian fit (dashed line) in curve b with a hole width, $\Gamma_{ZPH,}$ of ∼9.6 cm^{-1} provides the ET time of 1.1 ps (corrected for spectra resolution) in agreement with literature data.[40] For relatively broad ZPHs the read resolution correction is negligibly small. However, the much narrower ZPH shown in curve c in Figure 2B (ν_B = 10 953 cm^{-1}) is resolution limited. As a result, in this case the real ET must be slower than that estimated from the 3 cm^{-1} ZPH since the observed ZPH must be corrected for spectral resolution. Thus, the 3 cm^{-1} ZPH is resolution limited.

Regarding the transient holes obtained for the three single mutants shown in Figure 3, only the L131LH mutant clearly reveals a weak and narrow (∼6.5 cm^{-1}) ZPH that is not resolved in either the L160LH or M197FH mutants (other excitations are not shown for brevity), indicating a much stronger coupling with phonons and marker mode(s) in the L160LH and M197FH mutants. A comparison of the low-temperature resonant holes shown in Figures 2 and 3 indicates that CS kinetics, revealed via $P^+Q_A^-$ transient holes, varies from mutant to mutant. It is likely that the energetic asymmetry between the P_A and P_B molecules changes upon mutation leading to alteration of the charge-transfer character of the P-band (increasing el−ph coupling strength); the latter could also modify the ET time (vide infra). Theoretical description of these data is beyond the scope of this work. Note that spectra shown in Figure 4A reveal clear differences within the $P^{\bullet+}$ state(s) in the spectral region of 8 600−12 000 cm^{-1} indicating that H-bonds affect the spin density distributions of the primary donor cation radical $P^{\bullet+}$ in agreement with earlier data obtained by ENDOR and TRIPLE resonance experiments.[27] The largest difference is observed in the M160LH mutant, probably because its $P^{\bullet+}$ is characterized by the strongest asymmetric distribution of the unpaired electron, similar to that of heterodimer mutant, M202LH.[27] Comparison of spectra a and b′ (gray) in Figure 4B demonstrates that the P′-band is not related to the primary donor state P, as indicated by the absence of the transient bleach in this spectral region. It is also unlikely that the P′-band corresponds to the upper excitonic component (P_+) of the P-band.[41]

4.2. Persistent Holes. The satellite's hole structure observed in Figure 5A (ν_{B1} = 10 917 cm^{-1}) reveals higher energy bleaches as indicated by various arrows. Frame B shows expanded HB spectra from Figure 5A. However, the most striking features are (i) broad and significantly blue-shifted (∼320 cm^{-1}) antiholes (labeled for clarity in Figure 5B); (ii) weak red-shifted (∼150 cm^{-1}) antiholes (see Figure 5A/B); (iii) vibronic states indicated by upward arrows (near 580, 740, 1380, and 1630 cm^{-1}) likely originating from the coupling of high-frequency vibrations of BChls to the electronic transition within the P-band (the high-energy excitation states provide a local "bath" for the electronic degrees of freedom, and, as a result, they facilitate efficient downhill energy transfer to the special pair pigments); and (iv) the bleaches observed within the B and H bands (labeled by dashed arrows). The bleaches within the B and H bands (see curve c in Figure 5A) suggest connectivity of different absorption bands (states) since at 4 K only downward energy transfer is possible and the observed bleaches within the B and H bands are likely of excitonic origin. Note that, in the case of persistent holes, we do not have a contribution from the electrochromic shifts of pigments contributing to the B and H bands due to the absence of charge-separated state(s); thus, the coupling between the P, B, and H bands is more directly observed. However, the presence of large blue-shifted antiholes affecting the zero-order state energies will also modify the excitonic couplings complicating theoretical description of the persistent HB spectra. Besides, we cannot exclude the fact that protein conformational changes triggered by excitation of the P-band could also affect the properties of the other cofactors in the tightly packed bRC. In summary, data shown in Figure 5 suggest that vibrational frequencies mix with the electronic degrees of freedom, producing strong vibronic states. That is, the mixed exciton−vibrational states can then result in excitation delocalization over neighboring BChls even if pigments are separated by large energy gaps.[42,43]

Regarding the structure of the HB spectra discussed above, it is important to notice that the shapes of persistent and transient holes bleached within the P-band are significantly different (see Figures 2−6). This is, in part, because formation of charge-separated states in transient (photochemical) HB spectra produces additional electrochromic shifts of the zero-order state energies and, possibly, protein structural changes

DOI: 10.1021/acs.jpcb.9b08388
J. Phys. Chem. B 2019, 123, 8717−8726

that might also affect these zero-order state energies. In contrast, the analysis of persistent holes must take into account the presence of antihole(s), which, in general, can be observed at lower and higher frequencies, providing insight into the energy landscape within the P-band.[34] Large shifts of the antiholes observed in persistent holes are not surprising, as very different energy tiers have been observed in photosynthetic complexes; they typically occur on average near 5−20, 30−70, and 180−320 cm^{-1}.[44] However, we emphasize that resonant persistent holes observed above are bleached in a different subpopulation of bRCs in which CS times are much slower. Larger depths of the ZPHs observed in the persistent holes visibly reflect weaker el−ph couplings, as well as decreased couplings to the so-called marker mode(s) (vide infra). Theoretical description (beyond the scope of this work) will be necessary to understand the nature of persistent and transient bleaches within the P-band (research in progress).

4.3. On the Origin of the P′-Band. As mentioned above, comparison of spectra a and b′ in Figure 4B shows that P′-band does not burn transiently in a triple mutant. Most likely there is no efficient formation of the $P'^{+}Q_A^{-}$ state in this fraction of bRCs, meaning these bRCs have significantly longer excited state lifetimes (significantly slower CS times) leading preferentially to a bleach of persistent holes as shown in Figure 6. Resonant excitation of this fraction of bRCs (i.e., excitation within the P′-band) bleaches relatively deep broad persistent holes (see curve b in Figure 6A). The absence of ZPH in the latter spectrum is consistent with a stronger el−ph coupling in the primary electron donor in the subpopulation of bRCs associated with the P′-band. This is also consistent with data shown in frame A of Figure S3 in the Supporting Information (compare red and blue spectra burned at different fluences for λ_B = 488.0 nm (normalized at the maximum bleach of the P-band). These spectra also illustrate that the bleaches of the P and P′ bands are not correlated. Therefore, we conclude that the triple-mutant population is spectrally heterogeneous, and the bRCs with different spectral properties undergo charge separation at different rates and yield, in agreement with published time-domain data.[29,30] However, as revealed by the persistent bleaches, there are subpopulations of bRCs with the long-lived excited states that have been not revealed by time-domain spectroscopy. That is, these fractions do not form effectively the long-lived $P^{+}Q_A^{-}$ and $P'^{+}Q_A^{-}$ bottleneck states. The large blue shift (∼40 nm) of the P′-band (in comparison with the P-band) is also observed in the single M160LH mutant (Figure 3B). The shift could be associated with removal of the H-bond to the C_2 acetyl carbonyl group of P_A in a fraction (at least 25%) of bRCs. This is supported by the literature data for L168HF mutant, which lacks this particular H-bond, in which the P-band is also significantly blue-shifted in comparison to the wild type bRCs.[25] Moreover, a similar band between the P- and H-bands was also observed in deuterated bRC from *Rb. sphaeroides*, though never commented on.[37] Importantly, the P′-band has been never observed in freshly prepared bRCs from *Rb. sphaeroides*. The H-bond to His L168 in the L160LH mutant might be broken in a fraction of bRCs in comparison to the WT bRCs, as reflected by about 35−40% absorbance decrease of the P-band in this particular mutant when spectra were normalized for the integrated intensity of the H-band (see Figure S5 in the Supporting Information). However, in contrast to the triple mutant, there is a partial transient bleach of P′-band in M160LH. Thus, it is possible that a partial bleach of the P′-band in the single M160LH mutant is likely due to a stronger electron−vibrational coupling in the P-band. However, it cannot be excluded that partial bleach of the P′-band is due to a contribution from an upper excitonic component (P_+) of a mutation-modified special pair. In summary, we have demonstrated above that the three additional H-bonds to the special pair BChls in the triple mutant clearly affect the energy and excitonic structure of the first excited electronic state (P*) of P relative to the ground state. However, despite the large change in redox potential of P, all mutants (at least in the major fraction of bRCs) are capable of relatively fast ET as revealed by the resonant $P^{+}Q_A^{-}$ transient HB spectra.

4.4. On EET Transfer Process in Heterogeneous bRCs. Spectra shown in Figure 6 reveal the presence of a small subpopulation of triple-mutant RCs with slower EET from B_A to P. It is also possible that the average rate of EET from B_A to P is lower in the triple mutant due to the ∼60 cm^{-1} blue shift of the B_A maximum in the mutant compared to that in wild type bRC. The absence of a narrow ZPH under burning in the B_B band at 12 290 cm^{-1} (curve d in Figure 6A) shows that the EET from B_B to P is still very fast (on a subpicosecond time scale). Narrow ZPH (fwhm = 3−4 cm^{-1}) were observed under burning at frequencies between the H and B bands (12 910 cm^{-1}, depth = 12%; curve a in Figure 6A) and within the H_A band (13 090 cm^{-1}, depth = 4%; curve b in Figure 6B). This result was unexpected because it was previously observed that the energy transfer from the H to B bands was extremely fast in WT bRCs (100−200 fs).[7,45] Our HB data imply much slower EET times in the triple mutant (>4 ps). Closer inspection of HB spectra, burned at 12 910 and 13 090 cm^{-1} (curve d in panel B), shows that the maximum of the bleach in the P-band region is shifted by ∼200 cm^{-1} in comparison to the HB spectra produced at lower burning frequencies (compare spectra c/d and b in Figure 6A and 6B, respectively). Thus, a small subpopulation of triple-mutant RCs must exist in which EET transfer from the H- to the B-band is relatively slow, and a fraction of bRCs within the P-band must have absorption maximum significantly red-shifted compared to that in the major subpopulation. The same effects are observed in spectra b and c in Figure 6B. Namely, spectrum c was obtained for nonresonant excitation (λ_B = 488.0 nm) bleaching mostly the major population of bRCs with the minimum close to the maximum of the P-band. Curve d is very similar to the sum of spectra b and c (properly scaled; data not shown) since spectrum d was generated by simultaneous burning at 13 090 and 20 490 cm^{-1}. Finally, the HB spectra shown in Figure 6 also indicate that the P and P′ bands are not correlated.

4.5. Potential Energy Curves of PB_AH_A, $P^*B_AH_A$, and $P^{+}B_AH_A^{-}$ states. We demonstrated that the HB spectra discussed above (both transient and persistent) of the high P/P^+ midpoint potential L131LH + M160LH + M197FH mutant of *Rb. sphaeroides* provide new insight into mutation-induced perturbations (i.e., bRC heterogeneity) via formation of three additional H-bonds to the special pair BChls, P_A and P_B. The mutations mostly affect the energy and shape of both the P and B bands. Nonphotochemical (persistent) holes observed in the triple mutant are due to the presence of long-lived excited states. By comparing transient and persistent HB spectra, P* with a relatively fast ET time (observed via transient holes) is revealed to have a strong el−ph coupling strength, as well as strong coupling to the so-called marker mode(s). On the contrary, bRCs with long-lived excited states reveal much weaker coupling strength with phonons and marker mode(s).

DOI: 10.1021/acs.jpcb.9b08388
J. Phys. Chem. B 2019, 123, 8717−8726

Given that the marker mode (vibration at 100−150 cm^{-1}) is widely believed to be a reaction coordinate of initial electron transfer in bRCs,[46−49] we suggest that the coupling of the P → P* transition to this mode can affect ET rates. According to transient absorption data, the ET time in the triple mutant at low temperature is about 290 ps[29] and much slower than the vibrational relaxation time for the P* state.[47,50] Therefore, ET in the triple mutant proceeds nonadiabatically with an activation energy $E_A = \lambda/4(1 + \Delta G°/\lambda)^2$, where λ and $\Delta G°$ are the reorganization energy and free energy difference associated with this reaction. In what follows, we denote the first charge-separated state in the triple mutant as $P^+H_A^-$ because the $P^+B_A^-$ state may not be populated directly due to the 260 mV increase in midpoint potential of P in comparison with the energy levels observed in the WT bRC.[29,38]

In Figure 7, the positions of the potential energy surfaces of the $P^*B_AH_A$ and $P^+B_AH_A^-$ states are shown schematically

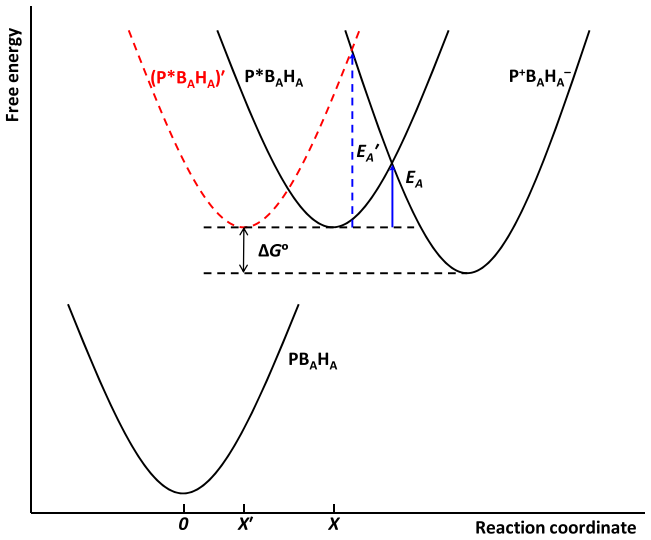

Figure 7. Schematic arrangement of potential energy curves of PB_AH_A, $P^*B_AH_A$, and $P^+B_AH_A^-$ states as a function of the reaction coordinate (X; a marker mode). The shifted $(P^*B_AH_A)'$ state corresponds to a P* state, characterized by a weaker coupling to the marker mode and phonons contributing to persistent holes burned within P.

relative to PB_AH_A as functions of a dimensionless reaction coordinate (X). The coupling strength (Huang−Rhys factor) of the P → P* transition is defined by the expression $S = 1/2X^2$.[51]

A decrease in the coupling strength for the transition would mean a decrease of the P^*B_A state potential energy, i.e., the shift of the $(P^*B_AH_A)'$ relative to the PB_AH_A ground state with a new equilibrium position X'. At the same time, the shift between reactant $(P^*B_AH_A)'$ and product $(P^+B_AH_A^-)$ states increases the activation energy (E_A') of the reaction, provided that the equilibrium position of the $P^+B_AH_A^-$ state is not altered, and decreases the rate of primary charge separation.[52] Thus, a decrease of coupling strength of the optical transition to the marker mode should lead to an increase of the reorganization energy of ET, as well as an increase of the activation energy of the ET reaction, thus decreasing the ET rate even if $\Delta G°$ is not changed. Interestingly, it was suggested earlier[53] that strong electron−phonon coupling for the P → P* transition makes ET rates less sensitive to the variance in $\Delta G°$ of the primary ET reaction. Since the observed persistent holes (burned within the P-band) are characterized by a relatively weak electron−phonon coupling, we conclude that in the triple mutant, the variance in coupling strength of the optical transition of P to phonons and especially to the marker mode(s), together with structural heterogeneity, is likely the origin of the dispersion in ET rates. In fact, the same may hold for the WT bRC of *Rb. sphaeroides* (though to a lesser extent), explaining the weak dispersive CS observed in the kinetics.[54]

This scheme also sheds light on the unusually fast ET rate of the M197FH mutant that is comparable to the ET rate of WT bRC.[55,56] The M197FH bRCs contain a single amino acid change of phenylalanine to histidine at M197 that results in the large increase of +125 mV in the P/P^+ midpoint potential.[26] To explain the fast rate despite the large change in potential, it was suggested that the mutation M197FH might also affect the midpoint potential of B_A, thus compensating for the increase of the midpoint potential of P.[56] Our data show a stronger coupling with phonons and marker mode(s) in the mutant compared to WT bRC (see panel C in Figure 3). Therefore, it is plausible that the stronger coupling with phonons and marker mode(s) partly compensates for the decrease in $\Delta G°$ of the primary ET reaction in the M197FH mutant.

5. CONCLUDING REMARKS

In summary, site-selective high-resolution transient $P^+Q_A^-$ and persistent HB spectra exposed differences in el−ph coupling strength, as well as a different coupling to the marker mode(s), which appear to affect the ET times. Transient holes are observed for fast (tens of picoseconds or faster) ET times, while the persistent holes are bleached in a fraction of at least 12% of the bRCs with long-lived excited states. These bRCs are characterized by much weaker el−ph coupling. We propose that a decrease of coupling strength of the optical transition to the marker mode should lead to an increase of the reorganization energy of ET, as well as an increase of the activation energy of the ET reaction, thus decreasing the ET rate even if $\Delta G°$ is not changed. In contrast to the WT bRC, low-temperature spectra obtained for the triple mutant and single (M160LH) mutants reveal a weak additional absorption band near 855 nm (referred to above as the P′ band) located between the P and B absorption bands. Its large blue shift (in comparison with the P-band) is most likely associated with removal of the H-bond to the C_2 acetyl carbonyl group of P_A in a small fraction (at least 25%) of bRCs. Much larger fraction of bRCs seems to be affected in the M160LH, though a small fraction of P′ is also observed in the triple mutant. Therefore, we suggest that in both triple and single L160LH mutants the H-bond to His L168 can be broken. However, much smaller fraction of bRCs with P′-band is observed in the triple mutant, most likely due to additional stabilization of the special pair BChls via the H-bonds between imidazole groups of His L131 and keto carbonyl groups of P_A and H-bond between His M197 and acetyl carbonyl group of P_B.

■ ASSOCIATED CONTENT

Supporting Information

The Supporting Information is available free of charge on the ACS Publications website at DOI: 10.1021/acs.jpcb.9b08388.

Absorption spectra of four mutants of *Rb. sphaeroides* in a broad spectral range, description of normalization of

DOI: 10.1021/acs.jpcb.9b08388
J. Phys. Chem. B 2019, 123, 8717−8726

transient nonresonant holes, nonresonant persistent holes burned (λ_B = 488.0 nm), fluence dependence of the hole depth burned at ν_B = 10 917 cm^{-1}, absorption spectra obtained for WT and M160LH mutant BRCs, and a direct comparison of spectra obtained for the triple bRC mutant (L131LH + M160LH + M197FH) and single M160LH mutant (PDF)

AUTHOR INFORMATION

Corresponding Author

*E-mail: ryszard@ksu.edu.

ORCID

James P. Allen: 0000-0002-7760-3921

Ryszard Jankowiak: 0000-0003-3302-9232

Present Address

[⊥]On leave from the Institute of Basic Biological Problems, Russian Academy of Sciences, Pushchino, Moscow Region 142290, Russia.

Notes

The authors declare no competing financial interest.

ACKNOWLEDGMENTS

This work was supported by the Chemical Sciences, Geosciences and Biosciences Division, Office of Basic Energy Sciences, Office of Science, U.S. Department of Energy (Grant No. DE-SC0006678 to R.J.) and National Science Foundation (CHE-1904860 to J.P.A. and J.C.W.). We acknowledge assistance with the reaction center preparations by Eduardo Espiritu and Kori Chamberlain.

REFERENCES

(1) Blankenship, R. E. *Molecular Mechanisms of Photosynthesis*; Wiley-Blackwell: Hoboken, NJ, 2002.

(2) Allen, J. P.; Feher, G.; Yeates, T. O.; Komiya, H.; Rees, D. C. Structure of the Reaction Center from *Rhodobacter sphaeroides* R-26: The Cofactors. *Proc. Natl. Acad. Sci. U. S. A.* **1987**, *84*, 5730−5734.

(3) *The Purple Phototrophic Bacteria*; Hunter, C. N., Daldal, F., Thurnauer, M. C., Beatty, J. T., Eds.; Advances in Photosynthesis and Respiration; Springer Netherlands: Dordrecht, 2009; Vol. *28*.

(4) Woodbury, N. W.; Allen, J. P. The Pathway, Kinetics and Thermodynamics of Electron Transfer in Wild Type and Mutant Reaction Centers of Purple Nonsulfur Bacteria. In *Anoxygenic Photosynthetic Bacteria*; Blankenship, R. E., Madigan, M. T., Bauer, C. E., Eds.; Advances in Photosynthesis and Respiration; Kluwer Academic Publishers: Dordrecht, 1995; Vol. *2*, pp 527−557.

(5) Kirmaier, C.; Holten, D. Electron Transfer and Charge Recombination Reactions in Wild-Type and Mutant Bacterial Reaction Centers. In *Photosynthetic Reaction Center*; Deisenhofer, J., Norris, J. R., Eds.; Academic Press: New York, 1993; pp 49−70.

(6) Wang, H.; Hao, Y.; Jiang, Y.; Lin, S.; Woodbury, N. W. Role of Protein Dynamics in Guiding Electron-Transfer Pathways in Reaction Centers from *Rhodobacter sphaeroides*. *J. Phys. Chem. B* **2012**, *116*, 711−717.

(7) Vos, M. H.; Breton, J.; Martin, J.-L. Electronic Energy Transfer within the Hexamer Cofactor System of Bacterial Reaction Centers. *J. Phys. Chem. B* **1997**, *101*, 9820−9832.

(8) Shuvalov, V. A.; Yakovlev, A. G. Coupling of Nuclear Wavepacket Motion and Charge Separation in Bacterial Reaction Centers. *FEBS Lett.* **2003**, *540*, 26−34.

(9) Ma, F.; Romero, E.; Jones, M. R.; Novoderezhkin, V. I.; Van Grondelle, R. Vibronic Coherence in the Charge Separation Process of the *Rhodobacter sphaeroides* Reaction Center. *J. Phys. Chem. Lett.* **2018**, *9*, 1827−1832.

(10) Konar, A.; Sechrist, R.; Song, Y.; Policht, V. R.; Laible, P. D.; Bocian, D. F.; Holten, D.; Kirmaier, C.; Ogilvie, J. P. Electronic Interactions in the Bacterial Reaction Center Revealed by Two-Color 2D Electronic Spectroscopy. *J. Phys. Chem. Lett.* **2018**, *9*, 5219−5225.

(11) Williams, J. C.; Alden, R. G.; Murchison, H. A.; Peloquin, J. M.; Woodbury, N. W.; Allen, J. P. Effects of Mutations near the Bacteriochlorophylls in Reaction Centers from *Rhodobacter sphaeroides*. *Biochemistry* **1992**, *31*, 11029−11037.

(12) Murchison, H. A.; Alden, R. G.; Allen, J. P.; Peloquin, J. M.; Taguchi, A. K.; Woodbury, N. W.; Williams, J. C. Mutations Designed to Modify the Environment of the Primary Electron Donor of the Reaction Center from *Rhodobacter sphaeroides*: Phenylalanine to Leucine at L167 and Histidine to Phenylalanine at L168. *Biochemistry* **1993**, *32*, 3498−3505.

(13) Nabedryk, E.; Allen, J. P.; Taguchi, A. K. W.; Williams, J. C.; Woodbury, N. W.; Breton, J. Fourier Transform Infrared Study of the Primary Electron Donor in Chromatophores of *Rhodobacter sphaeroides* with Reaction Centers Genetically Modified at Residues M160 and L131. *Biochemistry* **1993**, *32*, 13879−13885.

(14) Lapouge, K.; Näveke, A.; Gall, A.; Ivancich, A.; Seguin, J.; Scheer, H.; Sturgis, J. N.; Mattioli, T. A.; Robert, B. Conformation of Bacteriochlorophyll Molecules in Photosynthetic Proteins from Purple Bacteria. *Biochemistry* **1999**, *38*, 11115−11121.

(15) Lubitz, W.; Lendzian, F.; Bittl, R. Radicals, Radical Pairs and Triplet States in Photosynthesis. *Acc. Chem. Res.* **2002**, *35*, 313−320.

(16) Treynor, T. P.; Andrews, S. S.; Boxer, S. G. Intervalence Band Stark Effect of the Special Pair Radical Cation in Bacterial Photosynthetic Reaction Centers. *J. Phys. Chem. B* **2003**, *107*, 11230−11239.

(17) Allen, J. P.; Williams, J. C. Energetics of Cofactors in Photosynthetic Complexes: Relationship between Protein-Cofactor Interactions and Midpoint Potentials. In *The Biophysics of Photosynthesis*; Golbeck, J. H., van der Est, A., Eds.; Springer: New York, 2014; pp 275−299.

(18) Yakovlev, A. G.; Vasilieva, L. G.; Shkuropatov, A. Y.; Bolgarina, T. I.; Shkuropatova, V. A.; Shuvalov, V. A. Mechanism of Charge Separation and Stabilization of Separated Charges in Reaction Centers of Chloroflexus a Urantiacus and of YM210W(L) Mutants of *Rhodobacter sphaeroides* Excited by 20 fs Pulses at 90 K. *J. Phys. Chem. A* **2003**, *107*, 8330−8338.

(19) Yeates, T. O.; Komiya, H.; Chirino, A.; Rees, D. C.; Allen, J. P.; Feher, G. Structure of the Reaction Center from *Rhodobacter sphaeroides* R-26 and 2.4.1: Protein-Cofactor (Bacteriochlorophyll, Bacteriopheophytin, and Carotenoid) Interactions. *Proc. Natl. Acad. Sci. U. S. A.* **1988**, *85*, 7993−7997.

(20) Chirino, A. J.; Lous, E. J.; Huber, M.; Allen, J. P.; Schenck, C. C.; Paddock, M. L.; Feher, G.; Rees, D. C. Crystallographic Analyses of Site-Directed Mutants of the Photosynthetic Reaction Center from *Rhodobacter sphaeroides*. *Biochemistry* **1994**, *33*, 4584−4593.

(21) McAuley, K. E.; Fyfe, P. K.; Ridge, J. P.; Isaacs, N. W.; Cogdell, R. J.; Jones, M. R. Structural Details of an Interaction between Cardiolipin and an Integral Membrane Protein. *Proc. Natl. Acad. Sci. U. S. A.* **1999**, *96*, 14706−14711.

(22) Spiedel, D.; Roszak, A. W.; McKendrick, K.; McAuley, K. E.; Fyfe, P. K.; Nabedryk, E.; Breton, J.; Robert, B.; Cogdell, R. J.; Isaacs, N. W.; et al. Tuning of the Optical and Electrochemical Properties of the Primary Donor Bacteriochlorophylls in the Reaction Centre from *Rhodobacter sphaeroides*: Spectroscopy and Structure. *Biochim. Biophys. Acta, Bioenerg.* **2002**, *1554*, 75−93.

(23) Thielges, M.; Uyeda, G.; Cámara-Artigas, A.; Kálmán, L.; Williams, J. C.; Allen, J. P. Design of a Redox-Linked Active Metal Site: Manganese Bound to Bacterial Reaction Centers at a Site Resembling That of Photosystem II. *Biochemistry* **2005**, *44*, 7389−7394.

(24) Koepke, J.; Krammer, E.-M.; Klingen, A. R.; Sebban, P.; Ullmann, G. M.; Fritzsch, G. PH Modulates the Quinone Position in the Photosynthetic Reaction Center from *Rhodobacter sphaeroides* in the Neutral and Charge Separated States. *J. Mol. Biol.* **2007**, *371*, 396−409.

DOI: 10.1021/acs.jpcb.9b08388
J. Phys. Chem. B 2019, 123, 8717−8726

(25) Mattioli, T. A.; Lin, X.; Allen, J. P.; Williams, J. C. Correlation between Multiple Hydrogen Bonding and Alteration of the Oxidation Potential of the Bacteriochlorophyll Dimer of Reaction Centers from *Rhodobacter sphaeroides*. *Biochemistry* **1995**, *34*, 6142−6152.
(26) Lin, X.; Murchison, H. a.; Nagarajan, V.; Parson, W. W.; Allen, J. P.; Williams, J. C. Specific Alteration of the Oxidation Potential of the Electron Donor in Reaction Centers from *Rhodobacter sphaeroides*. *Proc. Natl. Acad. Sci. U. S. A.* **1994**, *91*, 10265−10269.
(27) Rautter, J.; Lendzian, F.; Schulz, C.; Fetsch, A.; Kuhn, M.; Lin, X.; Williams, J. C.; Allen, J. P.; Lubitz, W. ENDOR Studies of the Primary Donor Cation Radical in Mutant Reaction Centers of *Rhodobacter sphaeroides* with Altered Hydrogen-Bond Interactions. *Biochemistry* **1995**, *34*, 8130−8143.
(28) Reimers, J. R.; Hush, N. S. A Unified Description of the Electrochemical, Charge Distribution, and Spectroscopic Properties of the Special-Pair Radical Cation in Bacterial Photosynthesis. *J. Am. Chem. Soc.* **2004**, *126*, 4132−4144.
(29) Woodbury, N. W.; Lin, S.; Lin, X.; Peloquin, J. M.; Taguchi, A. K. W.; Williams, J. C.; Allen, J. P. The Role of Reaction Center Excited State Evolution during Charge Separation in a *Rb. sphaeroides* Mutant with an Initial Electron Donor Midpoint Potential 260 MV above Wild Type. *Chem. Phys.* **1995**, *197*, 405−421.
(30) Lin, S.; Lin, X.; Williams, J. C.; Taguchi, A. K. W.; Allen, J. P.; Woodbury, N. W. Reaction Center Heterogeneity Probed by Multipulse Photoselection Experiments with Picosecond Time Resolution. In *The Reaction Center of Photosynthetic Bacteria*; Michel-Beyerle, M. E., Ed.; Springer Berlin Heidelberg: Berlin, Heidelberg, 1996; pp 217−223.
(31) Ortega, J. M.; Mathis, P.; Williams, J. C.; Allen, J. P. Temperature Dependence of the Reorganization Energy for Charge Recombination in the Reaction Center from *Rhodobacter sphaeroides*. *Biochemistry* **1996**, *35*, 3354−3361.
(32) Paddock, M. L.; Rongey, S. H.; Feher, G.; Okamura, M. Y. Pathway of Proton Transfer in Bacterial Reaction Centers: Replacement of Glutamic Acid 212 in the L Subunit by Glutamine Inhibits Quinone (Secondary Acceptor) Turnover. *Proc. Natl. Acad. Sci. U. S. A.* **1989**, *86*, 6602−6606.
(33) Feng, X.; Neupane, B.; Acharya, K.; Zazubovich, V.; Picorel, R.; Seibert, M.; Jankowiak, R. Spectroscopic Study of the CP43′ Complex and the PSI−CP43′ Supercomplex of the *Cyanobacterium synechocystis* PCC 6803. *J. Phys. Chem. B* **2011**, *115*, 13339−13349.
(34) Jankowiak, R.; Reppert, M.; Zazubovich, V.; Pieper, J.; Reinot, T. Site Selective and Single Complex Laser-Based Spectroscopies: A Window on Excited State Electronic Structure, Excitation Energy Transfer, and Electron-Phonon Coupling of Selected Photosynthetic Complexes. *Chem. Rev.* **2011**, *111*, 4546−4598.
(35) Jankowiak, R.; Hayes, J. M.; Small, G. J. Spectral Hole-Burning Spectroscopy in Amorphous Molecular Solids and Proteins. *Chem. Rev.* **1993**, *93*, 1471−1502.
(36) Reddy, N. R. S.; Lyle, P. A.; Small, G. J. Applications of Spectral Hole Burning Spectroscopies to Antenna and Reaction Center Complexes. *Photosynth. Res.* **1992**, *31*, 167−194.
(37) Lyle, P. A.; Kolaczkowski, S. V.; Small, G. J. Photochemical Hole-Burned Spectra of Protonated and Deuterated Reaction Centers of *Rhodobacter sphaeroides*. *J. Phys. Chem.* **1993**, *97*, 6924−6933.
(38) Yakovlev, A. G.; Vasilieva, L. G.; Shkuropatov, A. Y.; Shuvalov, V. A. Coherent Phenomena of Charge Separation in Reaction Centers of LL131H and LL131H/LM160H/FM197H Mutants of *Rhodobacter sphaeroides*. *Biochemistry (Moscow)* **2011**, *76*, 1107−1119.
(39) Rancova, O.; Jankowiak, R.; Kell, A.; Jassas, M.; Abramavicius, D. Band Structure of the *Rhodobacter sphaeroides* Photosynthetic Reaction Center from Low-Temperature Absorption and Hole-Burned Spectra. *J. Phys. Chem. B* **2016**, *120*, 5601−5616.
(40) Woodbury, N. W.; Becker, M.; Middendorf, D.; Parson, W. W. Picosecond Kinetics of the Initial Photochemical Electron-Transfer Reaction in Bacterial Photosynthetic Reaction Centers. *Biochemistry* **1985**, *24*, 7516−7521.
(41) Reimers, J. R.; Biczysko, M.; Bruce, D.; Coker, D. F.; Frankcombe, T. J.; Hashimoto, H.; Hauer, J.; Jankowiak, R.; Kramer, T.; Linnanto, J.; et al. Challenges Facing an Understanding of the Nature of Low-Energy Excited States in Photosynthesis. *Biochim. Biophys. Acta, Bioenerg.* **2016**, *1857*, 1627−1640.
(42) Chin, A. W.; Prior, J.; Rosenbach, R.; Caycedo-Soler, F.; Huelga, S. F.; Plenio, M. B. The Role of Non-Equilibrium Vibrational Structures in Electronic Coherence and Recoherence in Pigment−Protein Complexes. *Nat. Phys.* **2013**, *9*, 113−118.
(43) Tiwari, V.; Peters, W. K.; Jonas, D. M. Electronic Energy Transfer through Non-Adiabatic Vibrational-Electronic Resonance. I. Theory for a Dimer. *J. Chem. Phys.* **2017**, *147*, 154308.
(44) Hofmann, C.; Aartsma, T. J.; Michel, H.; Kohler, J. Direct Observation of Tiers in the Energy Landscape of a Chromoprotein: A Single-Molecule Study. *Proc. Natl. Acad. Sci. U. S. A.* **2003**, *100*, 15534−15538.
(45) Lin, S.; Taguchi, A. K. W.; Woodbury, N. W. Excitation Wavelength Dependence of Energy Transfer and Charge Separation in Reaction Centers from *Rhodobacter sphaeroides*: Evidence for Adiabatic Electron Transfer. *J. Phys. Chem.* **1996**, *100*, 17067−17078.
(46) Vos, M. H.; Jones, M. R.; Hunter, C. N.; Breton, J.; Lambry, J. C.; Martin, J. L. Coherent Dynamics during the Primary Electron-Transfer Reaction in Membrane-Bound Reaction Centers of *Rhodobacter sphaeroides*. *Biochemistry* **1994**, *33*, 6750−6757.
(47) Yakovlev, A. G.; Shkuropatov, A. Y.; Shuvalov, V. A. Nuclear Wavepacket Motion Producing a Reversible Charge Separation in Bacterial Reaction Centers. *FEBS Lett.* **2000**, *466*, 209−212.
(48) Ma, F.; Romero, E.; Jones, M. R.; Novoderezhkin, V. I.; van Grondelle, R. Both Electronic and Vibrational Coherences Are Involved in Primary Electron Transfer in Bacterial Reaction Center. *Nat. Commun.* **2019**, *10*, 933.
(49) Eisenmayer, T. J.; De Groot, H. J. M.; Van De Wetering, E.; Neugebauer, J.; Buda, F. Mechanism and Reaction Coordinate of Directional Charge Separation in Bacterial Reaction Centers. *J. Phys. Chem. Lett.* **2012**, *3*, 694−697.
(50) Vos, M. H.; Rappaport, F.; Lambry, J.-C.; Breton, J.; Martin, J.-L. Visualization of Coherent Nuclear Motion in a Membrane Protein by Femtosecond Spectroscopy. *Nature* **1993**, *363*, 320−325.
(51) Parson, W. W. *Modern Optical Spectroscopy*; Springer Berlin Heidelberg: Berlin, Heidelberg, 2015.
(52) Hopfield, J. J. Electron Transfer between Biological Molecules by Thermally Activated Tunneling. *Proc. Natl. Acad. Sci. U. S. A.* **1974**, *71*, 3640−3644.
(53) Small, G. J.; Hayes, J. M.; Silbey, R. J. The Question of Dispersive Kinetics for the Initial Phase of Charge Separation in Bacterial Reaction Centers. *J. Phys. Chem.* **1992**, *96*, 7499−7501.
(54) Vos, M. H.; Lambry, J. C.; Robles, S. J.; Youvan, D. C.; Breton, J.; Martin, J. L. Direct Observation of Vibrational Coherence in Bacterial Reaction Centers Using Femtosecond Absorption Spectroscopy. *Proc. Natl. Acad. Sci. U. S. A.* **1991**, *88*, 8885−8889.
(55) Khmelnitskiy, A. Y.; Khatypov, R. A.; Khristin, A. M.; Leonova, M. M.; Vasilieva, L. G.; Shuvalov, V. A. Charge Separation in *Rhodobacter sphaeroides* Mutant Reaction Centers with Increased Midpoint Potential of the Primary Electron Donor. *Biochemistry (Moscow)* **2013**, *78*, 60−67.
(56) Wang, H.; Lin, S.; Allen, J. P.; Williams, J. C.; Blankert, S.; Laser, C.; Woodbury, N. W. Protein Dynamics Control the Kinetics of Initial Electron Transfer in Photosynthesis. *Science* **2007**, *316*, 747−750.

DOI: 10.1021/acs.jpcb.9b08388
J. Phys. Chem. B 2019, 123, 8717−8726